2014 International Conference on Unmanned Aircraft Systems (ICUAS)
May 27-30, 2014. Orlando, FL, USA

Explicit Model Identification and Control of a Micro Aerial Vehicle

Swee King Phang, Kun Li, Fei Wang, Ben M. Chen, Tong Heng Lee

Abstract— **In this work, we provide a nonlinear mathematical model identification methodology of an autonomous micro quadrotor, and the design of its orientation and position controllers. In the model identification, we specifically focus on the brushed D.C. motor dynamics, which further breaks down into three different segments: voltage generation, motor dynamics, and force/torque generation. Test bench experiments and software simulation are conducted to identify the parameters of the model derived from first principles physics model. Upon obtaining a good mathematical model of the micro quadrotor, model based orientation and position controllers are respectively implemented with linear quadratic regulator (LQR) and robust and perfect tracking (RPT) controller. The proposed control structure is designed and realized in a low cost micro quadrotor codenamed KayLion developed by the National University of Singapore.**

I. Introduction

The recent progress in sensory technology, processing unit and integrated actuators has realized smaller unmanned aerial vehicle (UAV) platforms with higher intelligence levels. These kind of platforms, commonly known as micro aerial vehicles (MAVs) make both military and civilian tasks possible, such as indoor navigation, search and rescue, surveillance and reconnaissance, as well as potential danger detection. These tasks require a self-stable system with its own navigation and obstacle avoidance capabilities in different environments.

However, based on a recent survey in [12], most commercial products of MAVs are not capable of carry powerful sensors and processors for autonomous flight. Due to the payload limitation, many of these small aircrafts do not have the endurance required for long-range missions. Most of the MAV platforms utilize ultra-light miniature sensors and Lithium-Polymer (Li-Po) batteries due to their light weight. As a result, relatively low-quality measurements and battery endurance limit the performance of the MAV in navigation and localization. A recent example sees a palm-sized gliding MAV developed by Harvard University weighing only 2 g and 10 cm in wing-span. It is capable of autonomous flight target sensing and obstacle avoidance using an optical flow sensor. Nevertheless, without any propulsion system, the platform is only able to glide with an initial thrust [16].

In MAV control and autonomous flight, a single camera as the sole position estimation sensor is preferred by most researchers [1], [5], [7], [9], [13]. The Vicon motion capturing system is also commonly used as a medium to provide accurate position measurements in a pre-setup environment [4], [10], [11]. In the work done by [6], a bio-inspired navigation method was adopted in MAVs equipped with optical flow microsensors. The MAV is able to take-off, land autonomously and perform collision avoidance with the proximity microsensors. However, the platform cannot vertically take-off and land (VTOL), resulting in limited application in cluttered environments. In the work documented in [15], a palm-sized co-axial helicopter is able to perform automatic take-off and landing, as well as target tracking using a camera. In [2], a 46 g quadrotor MAV is controlled with five optical flow sensors, each of which provides a 2-dimensional (2-D) optical flow measurement.

In our work, in order to verify the mathematical model and the control laws, a Vicon motion capturing system is set up to provide ground truth. This manuscript is an extension of research work done in previous publication in [8]. A more systematic break-down of the brushed D.C. motor dynamics is provided. With the accurate mathematical model identified, model based controllers can be designed and experimented with. The main contents of this paper are separated into six sections. The project will be introduced in Section I. Section II and section III briefly discuss the mathematical model, with a focus on kinematics and rigid-body dynamics. In section IV, an explicit model of the brushed D.C. motor used in the micro quadrotor is investigated. Section V describes the control schemes of the inner-loop and outer-loop controls. Pre-planned path tracking results are shown in the end of the section. Finally, concluding remarks are made in Section VI.

II. Nonlinear Mathematical Model Overview

In this section, a brief overview of the proposed nonlinear mathematical model will be discussed. It can be visualized in Fig. 1 where the inputs to the quadrotor system are the pulse width modulation (PWM) signals on four different channels, namely δ_{ail}, δ_{ele}, δ_{thr}, and δ_{rud}, while outputs of the system are the linear velocity (u,v,w) and position (x,y,z), angular velocity (p,q,r) and position (ϕ,θ,ψ).

Detailed derivation of each block in the overview figure can be found in our published manuscript in [8]. In this manuscript, we wish to propose an important improvement to our previously published model on motor dynamics. The focus of this paper will be on the model identification of the brushed D.C. motor system (highlighted in left dotted frame in Fig. 1), while the kinematics and 6 degree-of-freedom (DOF) rigid-body dynamics (in right dotted frame) will be

S. K. Phang is with the NUS Graduate School for Integrative Sciences & Engineering, National University of Singapore (NUS), Singapore. E-mail: king@nus.edu.sg

K. Li, B. M. Chen and T. H. Lee are with the Department of Electrical & Computer Engineering, National University of Singapore (NUS), Singapore. E-mail: {kunli89,bmchen,eleleeth}@nus.edu.sg

F. Wang is with the Temasek Laboratory, National University of Singapore (NUS), Singapore. E-mail: wangfei@nus.edu.sg

978-1-4799-2376-2/14/$31.00 ©2014 IEEE

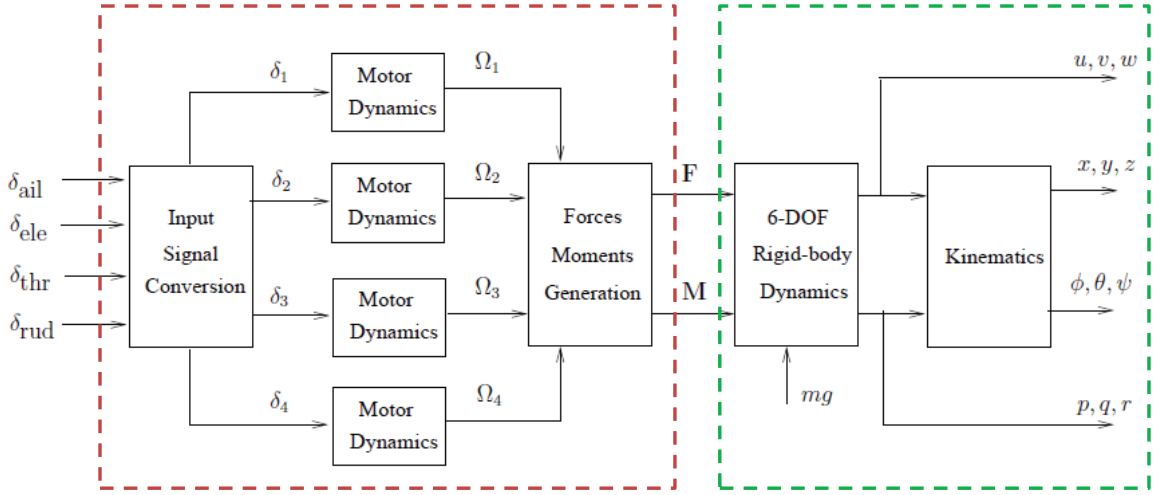

Fig. 1. Overview of mathematical model

briefly described in the next section to provide a better overall insight into this model.

III. Kinematics and 6-DOF Rigid-Body Dynamics

To obtain the translational and rotational motions between the North-East-Down (NED) and the body coordinate systems, one has the following well-known navigation equations [3]

$$\dot{\mathbf{P}}_\mathbf{n} = \mathbf{R}_{\mathbf{n/b}}\mathbf{V}_\mathbf{b} \quad (1)$$

$$\dot{\theta} = \mathbf{S}^{-1}\omega \quad (2)$$

where $\mathbf{P_n}$ is the position vector in the NED coordinate frame, $\mathbf{V_b}$ is the velocity vector in the body coordinate frame, θ is the Euler angle vector, and ω is the angular rate vector of the aircraft. Here, the rotational matrix, $\mathbf{R_{n/b}}$, and the lumped transformation matrix, $\mathbf{S}^{-1}$ are given by

$$\mathbf{R_{n/b}} = \begin{bmatrix} c_\theta c_\psi & s_\phi s_\theta c_\psi - c_\phi s_\psi & c_\phi s_\theta c_\psi + s_\phi s_\psi \\ c_\theta s_\psi & s_\phi s_\theta s_\psi + c_\phi c_\psi & c_\phi s_\theta s_\psi - s_\phi c_\psi \\ -s_\theta & s_\phi c_\theta & c_\phi c_\theta \end{bmatrix} \quad (3)$$

$$\mathbf{S}^{-1} = \begin{bmatrix} 1 & s_\phi t_\theta & c_\phi t_\theta \\ 0 & c_\phi & -s_\phi \\ 0 & s_\phi / c_\theta & c_\phi / c_\theta \end{bmatrix} \quad (4)$$

with $s_* = \sin(*)$, $c_* = \cos(*)$, and $t_* = \tan(*)$.

By using the Newton-Euler formalism which describes the translational and rotational dynamics of a rigid-body, the following two dynamics equations take into account of the mass of the quadrotor, m, and its inertia matrix, $\mathbf{J}$.

$$m\dot{\mathbf{V}}_\mathbf{b} + \omega \times (m\mathbf{V_b}) = \mathbf{F} + \mathbf{R_{n/b}}^{-1} mg\mathbf{z} \quad (5)$$

$$\mathbf{J}\dot{\omega} + \omega \times (\mathbf{J}\omega) = \mathbf{M} \quad (6)$$

where $\mathbf{F}$ and $\mathbf{M}$ are the force and moment vectors acting on the body.

IV. Brushed D.C. Motor Dynamics

The motor dynamics can be separated into 3 different blocks:

1) Voltage generation block: Analog voltage generated by the electronic speed controller (ESC) based on normalized PWM input;
2) Motor dynamics block: Speed dynamics of the motor powered by an input analog voltage;
3) Force and torque generation block: The force and torque produced by a single rotating propeller.

The following subsections will explicitly show the theoretical formulation and experimental verification of the model.

A. Equivalent Analog Voltage

In literature, most researchers assumed that the output voltage v_a, is directly driven by the normalized throttle signal δ to the ESC. However, this does not entirely represent the transformation caused by the ESC. In this work, it is experimentally determined that the supply voltage to the ESC does affect the performance of the motor.

Intuitively, one might assume that the output voltage from the ESC is directly proportional to the product of the normalized throttle signal and the supply voltage. This relationship depends on the circuitry of the ESC. In this work, the relationship between the inputs and the output is kept unknown, and will be identified next. In general, we can write it as

$$v_a = f(v_s, \delta) \quad (7)$$

where the PWM input is normalized as

$$\delta = \frac{u_{\text{PWM}} - 1039}{1000} \quad (8)$$

such that δ will always stay within 0 and 1. Here the u_{PWM} is the PWM input in unit μs.

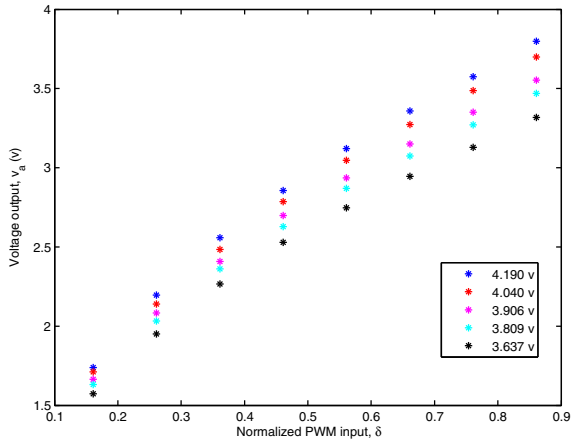

Fig. 2. Steady-state response of the ESC on two different inputs

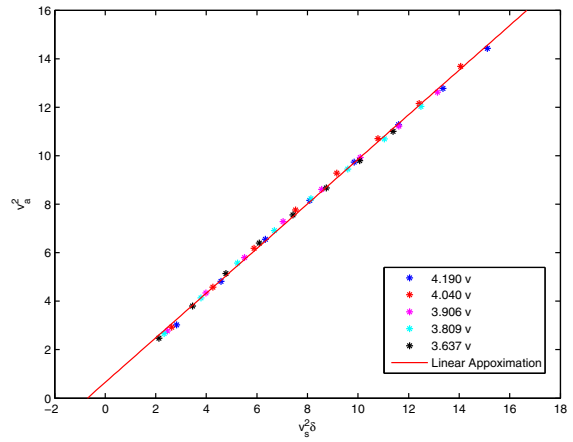

Fig. 3. Linear relationship of v_a^2 against $v_s^2\delta$ obtained experimentally

To determine the relationship between the supply voltage v_s and normalized throttle signal δ with the output voltage v_a, an experiment is performed by varying δ while measuring the output voltage from the ESC, v_a. The experiment is repeated with different v_s to the ESC. The results can be visualized in Fig. 2. Some manipulation was done to the input data and output data experimentally. Instead of plotting the output analog voltage against the normalized throttle input, we obtained a linear relationship between the product of normalized throttle input and supply voltage input, and the resultant analog voltage output as shown in Fig. 3. The identified equation is

$$v_a^2 = 0.9205 v_s^2 \delta + 0.6472 \tag{9}$$

B. Motor Dynamics

The main assumption made in deriving the motor model is that the mechanical friction is only linear to the motor speed; namely, only viscous friction is assumed to be present in the motor (such an assumption is approximate since Coulomb friction is usually experienced in motors). The motor dynamics can be separated into two parts, the electrical parts and the mechanical parts. The analysis on the motor system is also divided into dynamical analysis and steady-state analysis, as shown in the following list.

1) Electrical Properties: The rotor is assumed to be a single coil characterized by inductance L_a and resistance R_a, but the back EMF e, also has to be taken into account. The equation associated with such an electric circuit is given by

$$v_a(t) = L_a \frac{di_a}{dt} + R_a i_a + e \tag{10}$$

The following two equations hold for the back EMF e and the torque exerted by the motor T_M:

$$T_M = K_\Phi \Phi i_a \tag{11}$$
$$e = K_\Phi \Phi \Omega \tag{12}$$

where K_Φ is the magnetic flux constant, Φ is the magnetic flux, and Ω is the rotational speed of the rotor.

The flux Φ flowing through the motor is constant for a D.C. motor with constant stator magnet, we have

$$T_M = K_1 i_a \tag{13}$$
$$e = K_1 \Omega \tag{14}$$

where $K_1 = K_\Phi \Phi$.

2) Mechanical Properties: The motor exerts a torque while it is powered up. This torque acts on the mechanical structure, which is characterized by the rotor inertia J and the viscous friction coefficient F. Since the propeller is the only load to the motor, if Q is the propeller torque produced when spinning, the following equation describes the mechanical system of the motor:

$$T_M - Q = J\frac{d\Omega}{dt} + F\Omega \tag{15}$$

As Q is produced due to aerodynamic torque of the spinning propeller, it can be represented as

$$Q = k_Q \Omega^2 \tag{16}$$

More detail derivation of aerodynamic torque will be discussed in Section IV-C.

3) Dynamic Analysis: As seen above, the dynamics of the motor can be separated into electrical and mechanical dynamics. The electrical dynamics are given by

$$\frac{i_a(s)}{v_a(s) - e(s)} = \frac{K_a}{1 + \tau_a s} \tag{17}$$

where

$$K_a = \frac{1}{R_a}$$
$$\tau_a = \frac{L_a}{R_a}$$

are the rotor gain and time constant respectively.

The mechanical dynamic is in the similar form as it is given by

$$\frac{\Omega(s)}{T_M(s) - Q(s)} = \frac{K_m}{1 + \tau_m s} \tag{18}$$

where

$$K_m = \frac{1}{F}$$
$$\tau_m = \frac{J}{F}$$

are the mechanical gain and time constant respectively.

In general, as the electrical dynamic of the motor is much faster than the mechanical dynamic, i.e. $\tau_a << \tau_m$, the whole motor dynamic is assumed to behave as a first order system, with mechanical dynamic dominating the performance of the system. Thus, only τ_m needs to be identified here, while K_m will be broken down into more detail in Section IV-B.4.

An experiment is set up to estimate the value of τ_m. The time constant of such system can be approximated by measuring the transient response of the rotating speed of the motor given a step input. τ_m can then be obtained by finding the time taken from the beginning to 63.2% of the steady-state value. It is obtained as

$$\tau_m = 0.0821 \text{ s}$$

4) Steady-State Analysis: In modeling the whole quadrotor as a system, the dynamic of each motor is found to be much faster than the dynamic of the rigid-body, and thus the motor can be considered a static system. This will eases the identification work as the relationship between the speed of the motor to the input voltage of the motor can be obtained easily.

In equilibrium, taking all derivative terms of Equation (10) and (15) to zero, we have

$$v_a = R_a i_a + e \quad (19)$$
$$T_M = F\Omega + k_Q \Omega^2 \quad (20)$$

Combining Equation (13), (14), (19) and (20), we get

$$v_a = \left(\frac{R_a F}{K_1} + K_1\right)\Omega + \frac{R_a k_Q}{K_1}\Omega^2$$
$$\equiv K_2\Omega + K_3\Omega^2 \quad (21)$$

The steady-state coefficients of the motor, K_2 and K_3, can easily be identified in a test bench experiment. The motor is directly supplied with analog voltage v_a, and the corresponding rotational speed of the propeller is measured with a photo-interrupter. The result is plotted in Fig. 4. The response of the motor matches fairly well with the theoretical model of

$$v_a = K_2\Omega + K_3\Omega^2 \quad (22)$$

where

$$K_2 = 1.020 \times 10^{-3}$$
$$K_3 = 2.817 \times 10^{-7}$$

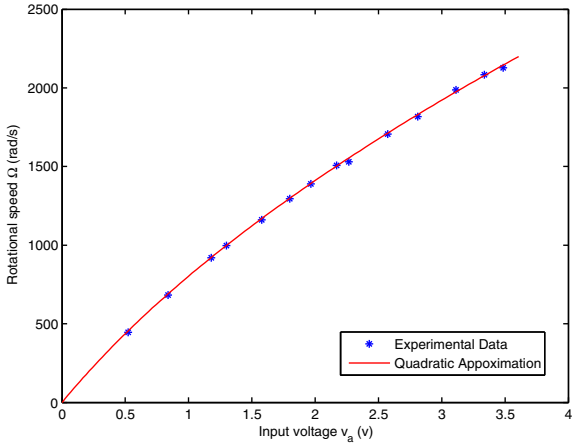

Fig. 4. Rotational speed response of the motor supplied with analog voltage

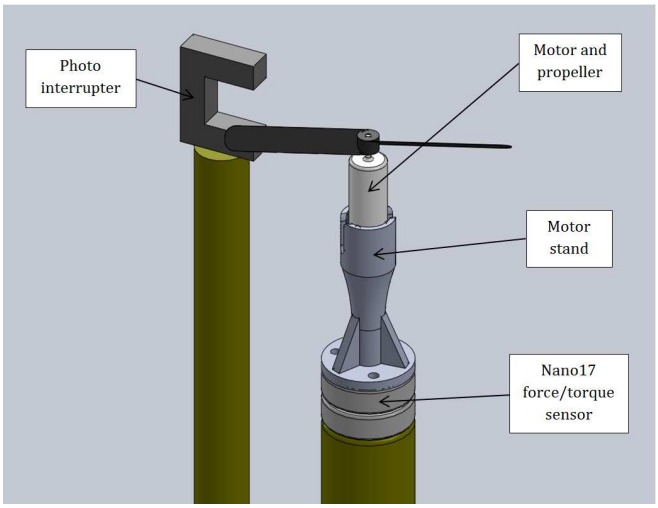

Fig. 5. Setup to obtain motor speed and thrust/torque produced

C. Force and Torque Produced

The forces and torques produced by the motors contribute to the forces and moments generated on aircraft's body-frame. For each of the rotating rotor, it creates a thrust, T, and a torque, Q. To differentiate thrust and torque produced by different motors, a subscript n will be added to the variable from this point onwards, where $n = 1,2,3,4$ corresponds to the rotor number. From the aerodynamics consideration, the thrust and torques created can be represented as

$$T_n = C_T \rho A r^2 \Omega_n^2 \quad (23)$$
$$Q_n = C_Q \rho A r^3 \Omega_n^2 \quad (24)$$

where C_T and C_Q are the aerodynamic coefficients of the propeller, ρ is the density of the air, A and r are the disc area swept by the rotating rotor and the radius of the rotor blade respectively. For a fixed pitch propeller, the aerodynamic coefficients are assumed constant as the pitch angle of the propeller is stationary. Thus, the equations can be simplified

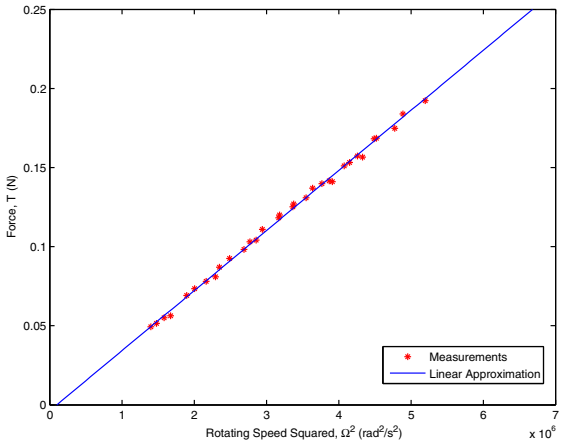

Fig. 6. Thrust vs rotation speed squared

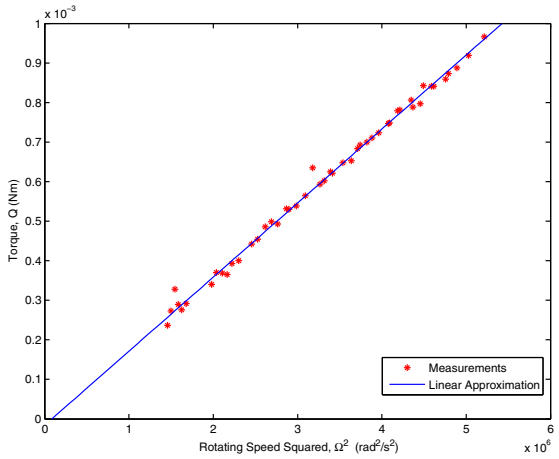

Fig. 7. Torque vs rotation speed squared

to

$$T_n = k_T \Omega_n^2 \quad (25)$$

$$Q_n = k_Q \Omega_n^2 \quad (26)$$

where k_T and k_Q can be obtained through an experiment setup as in Fig. 5. In this experiment, a high grade force and torque sensor is used. The Nano17 F/T Sensor from ATI Industrial Automation is the smallest commercially available 6-axis transducer in the market. It is designed to measure the 3 DOF force and 3 DOF torque in the small package of 17 mm diameter. With this product, accurate z-axis thrust and torque of the motor mounted on it can be obtained with ease. In the same setup, a photo interrupter is installed such that the spinning propeller passes through it. The time taken between each cut is recorded and the corresponding rotating speed can be calculated.

The results obtained are plotted in Fig. 6 and Fig. 7. The corresponding aerodynamic constants are the gradient of the plots, which are

$$k_T = 3.7901 \times 10^{-8} \text{ Ns}^2$$

$$k_Q = 1.8623 \times 10^{-10} \text{ Nms}^2$$

Next, the summation of thrusts produced by each of the rotor will result in a total thrust in body negative z-axis direction,

$$\mathbf{F} = \begin{bmatrix} 0 \\ 0 \\ -(T_1 + T_2 + T_3 + T_4) \end{bmatrix} \quad (27)$$

Pitch and roll moments will be generated by the thrust difference of the opposing rotors, while the yaw moment is generated based on the total moments of each rotors, provided they are installed strictly upright. The moment vector will then be

$$\mathbf{M} = \begin{bmatrix} \frac{l}{\sqrt{2}}(-T_1 + T_2 + T_3 - T_4) \\ \frac{l}{\sqrt{2}}(T_1 + T_2 - T_3 - T_4) \\ Q_1 - Q_2 + Q_3 - Q_4 \end{bmatrix} \quad (28)$$

where l is the length of quadrotor's beam given by

$$l = 0.0695 \text{ m}$$

V. Control

The above sections highlighted two important aspects in UAV model and control:

1) The kinematics and dynamics of the rigid-body are similar to most kind of UAVs. The only difference between the models of UAV systems and micro-quadrotor is that the body-frame forces and moments, is generated solely by four rotating motor in the latter. In this paper, we adopt a dual loop control structure, where the inner loop controls the orientation (or the moments) of the quadrotor, while the outer loop controls the position (or the forces) of the aircraft. Note that in position control, the z-direction is directly related to the forces produced by the motors, while the x- and y- directions control needs the aircraft to tilt its orientation to a specific set point to move. Thus, although a quadrotor has 6 DOF, the x- and y-rotational directions are strongly related to the x- and y-translational directions. We can then control the quadrotor with four inputs, namely the z-axis force, and the x-, y- and z-axes moments.
2) The relationship between the desired control inputs mentioned above can be easily back-traced from the identified equations of motor dynamics. Thus, we can generate the desired control inputs, then calculate and apply the normalized throttle input to each of the motors.

The basic control inputs to the system can be written as u_0 to u_3, where u_0 is the net desired body z-axis force of the quadrotor, while u_1 to u_3 are the desired body moments.

A. Orientation Control

The quadrotor orientation dynamics derived from Euler formalism shown in the previous sections can be summarized as

$$\dot{\phi} = p + q\sin\phi\tan\theta + r\cos\phi\tan\theta \quad (29)$$
$$\dot{\theta} = q\cos\phi - r\sin\phi \quad (30)$$
$$\dot{\psi} = q\frac{\sin\phi}{\cos\theta} + r\frac{\cos\phi}{\cos\theta} \quad (31)$$
$$J_x\dot{p} = u_1 + (J_y - J_z)rq \quad (32)$$
$$J_y\dot{q} = u_2 + (J_z - J_x)pr \quad (33)$$
$$J_z\dot{r} = u_3 + (J_x - J_y)pq \quad (34)$$

With feedback linearization input

$$u_1 = J_x\bar{u}_1 - (J_y - J_z)rq \quad (35)$$
$$u_2 = J_y\bar{u}_2 - (J_z - J_x)pr \quad (36)$$
$$u_3 = J_z\bar{u}_3 - (J_x - J_y)pq \quad (37)$$

we can approximate a linear system for each channel, given by

$$\begin{bmatrix}\dot{\phi}\\ \dot{p}\end{bmatrix} = \begin{bmatrix}0 & 1\\ 0 & 0\end{bmatrix}\begin{bmatrix}\phi\\ p\end{bmatrix} + \begin{bmatrix}0\\ 1\end{bmatrix}\bar{u}_1 \quad (38)$$
$$\begin{bmatrix}\dot{\theta}\\ \dot{q}\end{bmatrix} = \begin{bmatrix}0 & 1\\ 0 & 0\end{bmatrix}\begin{bmatrix}\theta\\ q\end{bmatrix} + \begin{bmatrix}0\\ 1\end{bmatrix}\bar{u}_2 \quad (39)$$
$$\begin{bmatrix}\dot{\psi}\\ \dot{r}\end{bmatrix} = \begin{bmatrix}0 & 1\\ 0 & 0\end{bmatrix}\begin{bmatrix}\psi\\ r\end{bmatrix} + \begin{bmatrix}0\\ 1\end{bmatrix}\bar{u}_3 \quad (40)$$

A model based controller can be designed to fulfill the stabilization tasks. Specifically, a linear quadratic regulator (LQR) is designed and implemented in the micro quadrotor. The flight test results will be shown in the next Section.

B. Position Control

To further investigate the performance of the micro quadrotor, a position controller is proposed. In order to realize this, a global position measurement needs to be obtained for feedback control. For this micro quadrotor, as it is designed for indoor navigation, no GPS sensor is installed in the system. In our solution, we utilize an external sensor source called the Vicon motion sensor installed on the wall of the building to provide an estimation of the UAV's local position in the building. The estimated measurement is accurate up to a bounded error of 0.1 mm.

By treating the closed inner loop and its command generator as a virtual actuator as proposed in [3], the outer-loop dynamics of the aircraft can be treated separately into 3 individual channels, namely the x-, y- and z-channels, without considering the coupling effect between the channels in the system. Thus in such situation, the dynamical equation of any one of the channel, say the x-channel, can be expressed as

$$\begin{bmatrix}\dot{x}_\mathrm{n}\\ \dot{u}_\mathrm{n}\end{bmatrix} = \begin{bmatrix}0 & 1\\ 0 & 0\end{bmatrix}\begin{bmatrix}x_\mathrm{n}\\ u_\mathrm{n}\end{bmatrix} + \begin{bmatrix}0\\ 1\end{bmatrix}a_{\mathrm{x,n}} \quad (41)$$

where $x_\mathrm{n}, v_\mathrm{n}, a_{\mathrm{x,n}}$ are the NED position, velocity and acceleration in x-direction respectively. By applying the robust and perfect tracking (RPT) approach introduced in [14], we can obtain an augmented system of the following form:

$$\dot{\mathbf{x}} = \mathbf{A}\mathbf{x} + \mathbf{B}\mathbf{u} + \mathbf{E}\mathbf{w} \quad (42)$$
$$\mathbf{y} = \mathbf{x} \quad (43)$$
$$\mathbf{e} = \mathbf{C_2}\mathbf{x} \quad (44)$$

where

$$\mathbf{x} = \begin{bmatrix}x_{\mathrm{n,r}}\\ u_{\mathrm{n,r}}\\ a_{\mathrm{x,n,r}}\\ x_\mathrm{n}\\ u_\mathrm{n}\end{bmatrix}, \quad \mathbf{w} = \dot{a}_{\mathrm{x,n,r}} \quad (45)$$

$$\mathbf{A} = \begin{bmatrix}0 & 1 & 0 & 0 & 0\\ 0 & 0 & 1 & 0 & 0\\ 0 & 0 & 0 & 0 & 0\\ 0 & 0 & 0 & 0 & 1\\ 0 & 0 & 0 & 0 & 0\end{bmatrix}, \quad \mathbf{B} = \begin{bmatrix}0\\ 0\\ 0\\ 0\\ 1\end{bmatrix}, \quad \mathbf{E} = \begin{bmatrix}0\\ 0\\ 1\\ 0\\ 0\end{bmatrix} \quad (46)$$

$$\mathbf{C}_2 = \begin{bmatrix}-1 & 0 & 0 & 1 & 0\end{bmatrix} \quad (47)$$

Here, state variables with subscript r represent the reference signals that the aircraft is tracking. With this configuration, we can obtain a closed-form solution for the state feedback gain for the system that solves the RPT control problem, given by

$$u = \mathbf{F}x \quad (48)$$

with

$$\mathbf{F} = \begin{bmatrix}-\dfrac{\omega_{n,x}^2}{\varepsilon_x^2} & -\dfrac{2\zeta_x\omega_{n,x}}{\varepsilon_x} & \dfrac{\omega_{n,x}^2}{\varepsilon_x^2} & \dfrac{2\zeta_x\omega_{n,x}}{\varepsilon_x} & 1\end{bmatrix} \quad (49)$$

where ε_x is the tuning parameter, $\omega_{n,x}$ and ζ_x are respectively the nominal natural frequency and damping ratio of the closed-loop system of x-axis dynamic. Using the same procedure, the controllers of the y- and z-channels are designed and implemented.

Fig. 8 and Fig. 9 show the performances of the MAV with the proposed control structure. Fig. 8 shows the MAV autonomous flight by tracking a square path while maintaining its height. Fig. 9 shows the MAV flight response to a zig-zag reference path. It can be seen that in both the figures, the performance of the MAV control is promising.

VI. Conclusion

In this paper, we have presented a systematic way of identifying the mathematical model of a micro quadrotor, specifically focusing on the D.C. motor dynamics, as it is the main contributer to the dynamics of the aircraft. The model identification of the motor dynamics is further separated into three parts, where each part were derived mathematically and verified with test bench experimental results.

Next, model based controllers were designed to control the orientation and the position of the MAV in a dual control loop structure. LQR controller was designed for inner-loop (orientation) control while RPT controller was

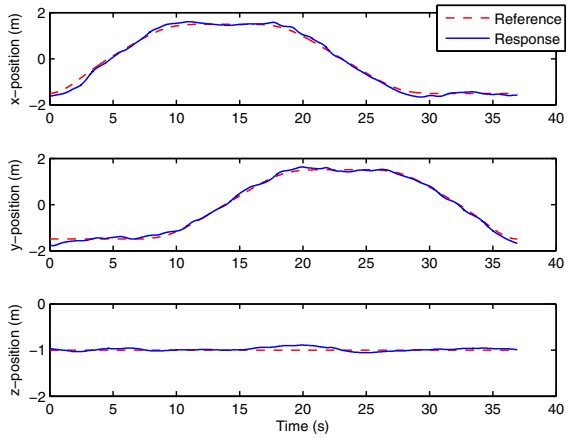

Fig. 8. Square path

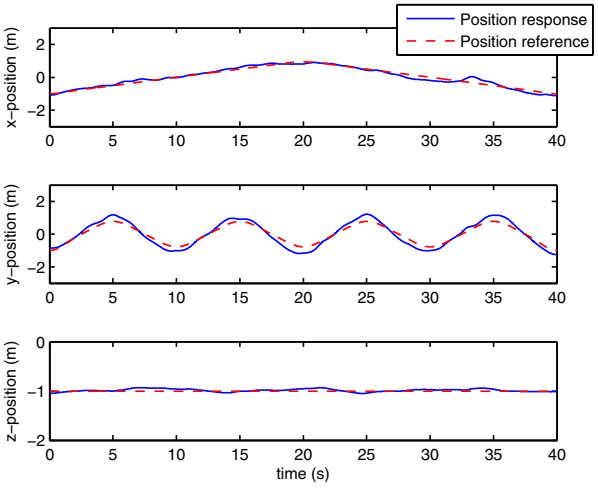

Fig. 9. Zig-zag path

designed for outer-loop (position) control. The controllers were realized in an ultra small quadrotor developed by the National University of Singapore, codenamed KayLion. Lastly, flight test results were shown to verify the proposed mathematical formulating and the controllers design.

REFERENCES

[1] S. Bouabdallah, P. Murrieri and R. Siegwart, "Towards autonomous indoor micro VTOL," *Autonomous Robots*, vol. 18, no. 2, pp. 171-183, 2005.

[2] A. Briod, J. C. Zufferey and D. Floreano, "Optic-flow based control of a 46g quadrotor," *Proc. Workshop on Vision-based Closed-Loop Control and Navigation of Micro Helicopters in GPS-denied Environments, IROS*, Tokyo, pp. 1-6, 2013.

[3] G. Cai, B. M. Chen and T. H. Lee, *Unmanned Rotorcraft Systems*, Springer, New York, 2011.

[4] R. Cory and R. Tedrake, "Experiments in fixed-wing UAV perching," *Proc. AIAA Guidance, Navigation, and Control Conf. and Exhibit*, Honolulu, Hawaii, pp. 7256-7267, 2008.

[5] S. M. Ettinger, M. C. Nechyba, P. G. Ifju and M. Waszak, "Vision-guided flight stability and control for micro air vehicles," *Proc. 2002 IEEE/RSJ Int. Conf. on Intelligent Robots and Systems*, Lausanne, vol. 3, pp. 2134-2140, 2002.

[6] W. E. Green, P. Y. Oh and G. Barrows, "Flying insect inspired vision for autonomous aerial robot maneuvers in near-earth environments," *Proc. 2004 IEEE Int. Conf. on Robotics and Automation*, New Orleans, LA, vol. 3, pp. 2347-2352, 2004.

[7] A. S. Huang, A. Bachrach, P. Henry, M. Krainin, D. Maturana, D. Fox and N. Roy, "Visual odometry and mapping for autonomous flight using an RGB-D camera," *Proc. Int. Symp. on Robotics Research (ISRR)*, Flagstaff, Arizona, pp. 1-16, 2011.

[8] K. Li, S. K. Phang, B. M. Chen and T. H. Lee, "Platform design and mathematical modeling of an ultralight quadrotor micro aerial vehicle," *Proc. 2013 Int. Conf. on Unmanned Aircraft Systems*, Atlanta, GA, pp. 1077-1086, 2013.

[9] L. Meier, P. Tanskanen, L. Heng, G. H. Lee, F. Fraundorfer and M. Pollefeys, "PIXHAWK: a micro aerial vehicle design for autonomous flight using onboard computer vision," *Autonomous Robots*, vol. 33, no. 1, pp. 21-39, 2012.

[10] D. Mellinger, M. Nathan and V. Kumar, "Trajectory generation and control for precise aggressive maneuvers with quadrotors," *The Int. Journal of Robotics Research*, vol. 31, no. 5, pp. 664-674, 2012.

[11] N. Michael, D. Mellinger, Q. Lindsey and V. Kumar, "The grasp multiple micro-uav testbed," *IEEE Robotics & Automation Magazine*, vol. 17, no. 3, pp. 56-65, 2010.

[12] D. J. Pines, and F. Bohorquez, "Challenges facing future micro-air-vehicle development," *Journal of Aircraft*, vol. 43, no. 2, pp. 290-305, 2006.

[13] F. Ruffier, S. Viollet, S. Amic and N. Franceschini, "Bio-inspired optical flow circuits for the visual guidance of micro air vehicles," *Proc. 2003 Int. Symp. on Circuits and Systems*, Bangkok, vol. 3, pp. 846-849, 2003.

[14] B. Wang, X. Dong, B. M. Chen, T. H. Lee and S. K. Phang, "Formation flight of unmanned rotorcraft based on robust and perfect tracking approach," *Proc. 2012 American Control Conf.*, Montreal, pp. 3284-3290, 2012.

[15] W. Wang, G. Song, K. Nonami, M. Hirata and O. Miyazawa, "Autonomous control for micro-flying robot and small wireless helicopter xrb," *Proc. 2006 IEEE/RSJ Int. Conf. on Intelligent Robots and Systems*, Beijing, pp. 2906-2911, 2006.

[16] R. J. Wood, S. Avadhanula, E. Steltz, M. Seeman, J. Entwistle, A. Bachrach, G. Barrows and S. Sanders, "An autonomous palm-sized gliding micro air vehicle," *IEEE Robotics & Automation Magazine*, vol. 14, no. 2, pp. 82-91, 2007.